

Glycobiology

2011, Volume 21, Issue 6, Pages 781-795

<http://dx.doi.org/10.1093/glycob/cwr002>

© The Author 2011. Published by Oxford University Press. All rights reserved.

Archimer
<http://archimer.ifremer.fr>

Effects of a sulfated exopolysaccharide produced by *Altermonas infernus* on bone biology

C Ruiz Velasco^{2,3}, M Baud'huin^{2,3}, C Sinquin⁴, M Maillason⁵, D Heymann^{2,3,6}, S Collic-Jouault⁴ and M Padrines^{1,2,3,*}

² INSERM U957, Faculté de Médecine, Université de Nantes, 1 rue Gaston Veil, Nantes cedex 01 F-44035, France

³ Laboratoire de Physiopathologie de la Résorption Osseuse et Thérapie des Tumeurs Osseuses Primitives, Université de Nantes, Nantes Atlantique Universités, EA3822, Nantes F-44035, France

⁴ Laboratoire de Biotechnologie et Molécules Marines, Département Biotechnologies Marines, BIOMAR, IFREMER, Nantes F-44311, France

⁵ IFR26–Ouest genopole, INSERM U892, Nantes F-44035 France

⁶ Centre Hospitalier Universitaire de Nantes, Nantes, France

* : Corresponding author : M. Padrines, Tel: +33-240-412-846; Fax: +33-240-412-860; e-mail: marc.padrines@univ-nantes.fr

Abstract:

The growth and differentiation of bone cells is controlled by various factors, which can be modulated by heparan sulfates. Here, we investigated the effects of an oversulfated exopolysaccharide (OS-EPS) on the bone. We compared the effect of this compound with that of a native EPS. Long-term administration of OS-EPS causes cancellous bone loss in mice due, in part, to an increase in the number of osteoclasts lining the trabecular bone surface. No significant difference in cancellous bone volume was found between EPS-treated mice and age-matched control mice, underlying the importance of sulfation in trabecular bone loss. However, the mechanism sustaining this osteoporosis was unclear. To clarify OS-EPS activities, we investigated the effect of OS-EPS on osteogenesis. Our results demonstrated that OS-EPS inhibited osteoclastogenesis in two cell models. Using the surface plasmon resonance technique, we revealed that OS-EPS can form a hetero-molecular complex OS-EPS/receptor activator of NF- κ B ligand (RANKL)/RANK and that RANK had a higher affinity for RANKL pre-incubated with OS-EPS than for RANKL alone, which would be in favor of an increase in bone resorption. However, in vitro, OS-EPS inhibited the early steps of osteoclast precursor adhesion and therefore inhibited the cell fusion step. In addition, we showed that OS-EPS reduced proliferation and accelerated osteoblastic differentiation, leading to strong inhibition of mineralized nodule formation, which would be in favor of an increase in bone resorption. Taken together, these data show different levels of bone resorption regulation by EPSs, most of them leading to proresorptive effects.

Keywords: bone metabolism bone remodeling exopolysaccharide glycosaminoglycan heparin

1. Introduction

Bone is a specialized connective tissue that is continually remodelled according to physiological events. This remodelling is the result of the activities of many cell lineages including mainly osteoblasts, osteocytes and osteoclasts. Their cell interactions control their cell activities and bone remodelling intensity. These interactions can be established either through cell–cell contact or by the release of many polypeptidic factors and/or their soluble receptor chains (cytokines, growth factors). These factors can act directly on osteogenic cells and their precursors to control differentiation, formation and functions (e.g. matrix formation, mineralization, resorption) (Kwan Tat *et al.*, 2004). Of these factors, proteoglycans (PGs) appear critical for maintaining an appropriate number of osteoblasts and osteoclasts by modulating their proliferation and/or differentiation (Lamoureux *et al.*, 2007).

PGs are composed of a core protein with covalently attached glycosaminoglycan (GAG) chains. These GAGs, linear polymers of repeated disaccharidic units, are sulphated and the number and position of the sulphates are extremely variable in sulphated GAGs, depending on the tissue, cell, and metabolic context, ensuring structural variability in these polysaccharides (Bernfield, 1999). These PGs are ubiquitous, being present as cell surface molecules anchored in the plasma membrane, as components of the insoluble extracellular matrix or as soluble molecules present in the extracellular matrix and serum. PGs function in both cell–cell and cell–extracellular matrix adhesion and can also act to promote the assembly of extracellular matrix molecules. Additionally, PGs bind to a wide range of bioactive molecules, such as growth factors and chemokines, which regulate cell behaviour in normal and pathological processes. Thus, the PGs or GAGs associated with the cell membrane or resident in the extracellular bone matrix regulate bone growth and remodelling (Ruiz Velasco *et al.*, 2010).

The osteoprotegerin (OPG)/Receptor Activator of the NF- κ B (RANK)/RANK Ligand (RANKL) molecular triad has been identified as a member of a ligand-receptor system that directly regulates osteoclast differentiation and osteolysis (Simonet *et al.*, 1997). While RANKL is a powerful inducer of bone resorption through its interaction with RANK (Kong *et al.*, 1999), OPG acts as a decoy receptor for RANKL, thereby strongly inhibiting osteoclast differentiation (Yasuda *et al.*, 1998). Any dysregulation in their respective expression leads to pathological conditions (Wittrant *et al.*, 2004). OPG contains a heparin-binding domain and strongly binds to GAGs with a high affinity (K_D : 0.28 nM for heparin) (Theoleyre *et al.*, 2006). PGs therefore decrease the bioavailability of OPG, inducing its internalization (Standal *et al.*, 2002, Kwan Tat *et al.*, 2006), and enhance the RANKL half-life at the cell membrane (Kwan Tat *et al.*, 2006). Like OPG, PGs interact with RANKL and abolish osteoclastogenesis (Shinmyouzu *et al.*, 2007). These data demonstrate that PGs must be considered as essential co-factors modulating bone remodelling. PGs are thus not simply passive structural components of cells and extracellular matrices, but instead multifunctional molecules that regulate cell behaviour by fine tuning the function of many regulatory proteins (Lamoureux, 2009).

Heparin has several kinds of biological activity, binding to various extracellular molecules. However, the role of heparin in the biological activity of bone remains unclear. Recently, Ariyoshi *et al.* (2008) showed that heparin suppressed osteoclastogenesis. In contrast, Irie *et al.* (2007) showed that heparin enhanced osteoclastic bone resorption by inhibiting OPG activity. Long-term heparin treatment causes cancellous bone loss in rats due in part to an increase in the number of osteoclasts lining the trabecular bone surface. However, the results from various other groups suggest that GAGs, and in particular heparan sulphate (HS) and heparin, are potent co-stimulators of osteogenic signalling pathways (Zhao *et al.*, 2006; Jackson *et al.*, 2007; Ling *et al.*, 2010)). Thus, the opportunity arises to leverage the stimulatory properties of HS-derived compounds as adjuvants for osteo-inductive therapies. However, the strong anticoagulant property limits applicability in other therapeutic indications. A further disadvantage of heparins is their animal origin and the increasing demand for heparins is in conflict with the limited resources.

A broad range of polysaccharides has emerged as an important class of bioactive products (Franz and Alban, 1995; Bernas, 2003; Mayer and Lehmann, 2001). Polysaccharide-producing marine microorganisms occur widely in nature in different types of habitat (Sutherland, 1996), and certain thermophilic and mesophilic polysaccharide-producing strains have been isolated from deep-sea hydrothermal vents (Guezennec, 2002; Nichols *et al.*, 2005). *Alteromonas infernus*, classified as a non-pathogenic microorganism by the Institut Pasteur, secretes a water-soluble acidic heteropolysaccharide (Raguénès *et al.*, 1997). The composition of this high-molecular-weight polysaccharide (10^6 g/mol) differs in monosaccharide content and/or ratio and sulphate content (10%) from other polysaccharides isolated from deep-sea hydrothermal bacteria and from polysaccharides of

other origins. Structural characterization has shown that this exopolysaccharide is a highly branched acidic heteropolysaccharide composed of neutral sugars (glucose, galactose) and uronic acids (glucuronic acid and galacturonic acid) (Roger *et al.*, 2004). The high-molecular-weight exopolysaccharide was chemically depolymerised and sulphated, with a view to obtaining a bioactive compound compatible with therapeutic use (Roger *et al.*, 2004). Highly sulphated low molecular-weight exopolysaccharide (40% sulphate groups, MW: 24,000, Fig. 1), with uronic acid and sulphate content comparable to that of heparin, was obtained without altering the sugar composition of this polymer (Guezennec *et al.*, 1998). In contrast to the exopolysaccharide secreted by *Alteromonas infernus*, this oversulphated exopolysaccharide (OS-EPS) has anticoagulant properties, a heparin-like activity. It is less potent than low-molecular-weight heparin and unfractionated heparin (2.5 and 6.5 times, respectively), and should therefore carry a lower risk of bleeding (Collic-Jouault *et al.*, 2001). Like heparin, OS-EPS increases the angiogenic properties of FGF-2 (Fibroblast growth factors-2) or VEGF (Vascular endothelial growth factor); however it also inhibits the effect of FGF-2-induced cell migration (Matou *et al.*, 2005). These angiogenic properties of OS-EPS are related to its sulphate content because no effect was observed with the native low molecular-weight exopolysaccharide (EPS). FGFs also play a major role in controlling cell proliferation, differentiation, and survival in several tissues, including bone (Marie, 2003). However, no data concerning the structure and biological activity of these exopolysaccharides on bone cell proliferation and differentiation were available until now. To explore its ability to promote bone resorption or formation, the influence of OS-EPS on bone cell proliferation and differentiation was determined. OE-EPS was compared with EPS in order to study the effect of sulphate content on the biological properties of the exopolysaccharide.

2. Results

2.1. OS-EPS inhibits the proliferation of BMSCs during osteoblastic differentiation

To study the effect of OS-EPS on osteoblast precursors, we used the bone marrow stem cell (BMSCs) model, in which dexamethasone is known to induce osteoblast differentiation. Proliferation of BMSCs during osteoblastic differentiation was analyzed in the presence of OS-EPS. 25 µg/mL of OS-EPS significantly inhibited cell proliferation (Fig. 2A and 2B) in contrast to EPS. To determine whether these effects were due to inhibition of cell proliferation and/or induction of cell death, we used time-lapse microscopy to monitor the mitosis events. The results demonstrated a 70% inhibition of cell mitosis in the presence of 25µg/mL of OS-EPS after 48 h of culture as compared to the control (Fig. 2C). To determine whether the OS-EPS induced death in BMSCs by apoptosis, Hoechst staining and caspase-3 activation were investigated. Hoechst staining showed no modification in nuclear morphology in the presence of OS-EPS as compared to control cells (data not shown). Concerning the caspase-3 activity in BMSCs, the results showed that OS-EPS did not induce any activation of caspases (not shown). Flow cytometry of DNA content was performed to identify cell cycle perturbations following treatment with OS-EPS over a 48-h period in BMSCs. Although 24 h of OS-EPS treatment did not modulate the cell cycle in BMSCs (data not shown), 48 h of OS-EPS treatment induced cell cycle arrest in G1 phases (Fig. 2D). The number of cells in G1 phases increased from 73 ± 2 to 83 ± 3 % when treated with OS-EPS (Fig. 2D). This observation was concomitant with a reduction in cells in S and G2/M phases: 25 ± 3 versus 17 ± 2 % (Fig. 2D). EPS had no effect in any of the experimental conditions, highlighting the importance of the sulphated polysaccharide on proliferation.

2.2. OS-EPS inhibits mineralized nodule formation in pre-osteoblasts

To examine the role of OS-EPS in extracellular matrix mineralization in BMSC cultures, BMSCs were treated for 17 days with OS-EPS, after which the mineral was visualized with von Kossa staining. As shown in Fig. 3A, OS-EPS dose-dependently inhibited mineralization with maximal inhibition occurring at 50 µg/mL. In BMSC cultures, OS-EPS reduced the formation of bone nodules. To further understand the mechanism by which OS-EPS inhibits mineralization, the cultures were treated with 25 µg/mL OS-EPS on days 3–17. OS-EPS reduced the formation of bone nodules when added in the first two weeks (D3 → D14) but not later (D17) (Fig. 3B). This result shows that OS-EPS is effective during

the osteoblast differentiation period (D3→D14), suggesting that OS-EPS blocks culture mineralization mainly by adversely affecting osteoblast differentiation and matrix depositing during the early matrix assembly stage and not by direct binding to hydroxyapatite crystals during the mineralization stage.

Based on reduced mineralization, it was expected that OS-EPS would reduce expression of osteoblastic markers in cells. This study was performed on BMSCs under conditions where runt-related transcription factor 2 (Runx2), alkaline phosphatase (ALP) and type I collagen expression (Col1 α 1) were observed by preosteoblast stage, followed by bone sialoprotein (BSP) and osteocalcin (OC) by mature osteoblast stage. Unexpectedly, after 17 days of treatment, OS-EPS induced BSP and OC (the mature osteoblast stage) in a dose-dependent manner (Fig. 3C). In contrast, OS-EPS reduced ALP, Runx2 and coll α 1 mRNA levels (preosteoblast stage) in a dose-dependent manner (Fig. 3C). This result clearly demonstrated that OS-EPS had an effect on osteoblastic differentiation. OS-EPS acted in the early stages of the process by affecting the preosteoblasts and accelerating osteoblastic differentiation.

These results suggest that OS-EPS led to significant inhibition of mineralized nodule formation that could be in favour of an increase in bone resorption. As RANKL is considered to be a powerful stimulator of bone resorption produced by mature osteoblasts, we also examined the effect of OS-EPS on RANKL expression by these cells. Figure 3D show that OS-EPS did not modulate the RANKL expression.

2.3. OS-EPS inhibits RANKL-induced osteoclastogenesis in human models

CD14⁺ cells are human monocyte cells which can differentiate into tartrate-resistant acid phosphatase (TRAP)-positive multinucleated cells in 21 days with RANKL stimulation. As shown in Figure 4A, in contrast to EPS, adding 0.5 μ g/ml of OS-EPS, at the same time as the RANKL was added, almost completely inhibited RANKL-induced osteoclastogenesis ($p < 0.01$). We confirmed this effect in a second model for osteoclastogenesis. RAW 264.7 cells are murine monocyte/macrophage cells which can differentiate into TRAP-positive multinucleated cells in 5 days with RANKL stimulation. OS-EPS completely inhibited RANKL-induced osteoclastogenesis in RAW 264.7 (Fig. 4B). To better characterize the mechanisms by which OS-EPS inhibits osteoclast formation, the effect of OS-EPS was assessed at different times in the culture period. When OS-EPS was added to the culture 3 days before RANKL (D-3), no osteoclasts were generated after 17 days (Fig. 4A) and the number of adherent CD14⁺ osteoclast precursors was lower than in the control condition. To determine whether these effects were due to induced loss of adhesion, the effects of OS-EPS were evaluated by counting viable cells, as assessed by trypan blue exclusion. After the adherence of CD14⁺ cells in the wells, these cells were incubated with EPS or OS-EPS for 5 days. Blue trypan counting revealed that OS-EPS caused a loss of adherence in this type of cell (Fig. 4C). In this culture condition, fewer osteoclast precursors thus adhered to the plastic surface and less osteoclasts were generated in the presence of RANKL. The addition of OS-EPS after one week of the culture stage (D7) did not completely inhibit osteoclast formation (Figure 4A). OS-EPS acted at two distinct levels of osteoclastogenesis: i) in the early stages of the process by affecting and decreasing cell adherence and ii) at the end of the osteoclastogenesis process by inhibiting the spreading of the preformed osteoclasts. This result clearly demonstrated that OS-EPS had an effect on RANKL-induced osteoclastogenesis. OS-EPS acted in the early stages of the process by affecting and decreasing cell adherence.

2.4. OS-EPS binds to RANKL

OPG/RANK and RANKL have been identified as members of a ligand-receptor system that directly regulates osteoclast differentiation and osteolysis. While RANKL is a powerful inducer of bone resorption through its interaction with RANK, OPG is a soluble decoy receptor and acts as a strong inhibitor of osteoclastic differentiation.

Surface plasmon resonance (SPR)-binding assays showed that recombinant full length OPG binds immobilized heparin (Theoleyre *et al.*, 2006). To determine the involvement of OS-EPS in the binding of OPG, we determined the kinetic parameters by injecting different concentrations of OS-EPS over immobilized OPG and thus demonstrated the high-affinity OPG binding to OS-EPS (dissociation constant K_D : 0.22 nM) (Fig. 5). To explore the molecular mechanism underlying the effect of OS-EPS on RANKL-induced osteoclastogenesis, we investigated the molecular interactions between RANKL and OS-EPS by SPR. Surprisingly, OS-EPS was also able to bind to immobilized-RANKL, whereas EPS was not (Fig. 5A). We next compared OS-EPS activity to that of heparin, heparan sulphate, chondroitin sulphate and dermatan sulphate. None of the GAGs analyzed were able to bind to RANKL, with the exception of OS-EPS (Fig. 5A). Furthermore, using a single cycle kinetic assay, the K_D of OS-EPS for RANKL was 91 pM (Fig. 5).

As RANKL is the natural ligand of RANK, we wondered whether OS-EPS could inhibit the RANKL–RANK complex present at the osteoclast membrane. We investigated the molecular interactions between OS-EPS, RANKL and RANK using the SPR technique. We confirmed that RANK or RANKL bound to immobilized RANKL or immobilized RANK, respectively (Fig. 5B and 5C). While, in our conditions, OS-EPS did not bind to immobilized RANK (Fig. 5C), it bound to the preformed RANKL/RANK complex (Fig. 5B) thereby forming a ternary complex OS-EPS/RANKL/RANK. In addition, the pre-incubation of OS-EPS (30 min at room temperature) with RANK or RANKL did not inhibit the capacity of OS-EPS to further bind to the preformed ternary complex OS-EPS/RANKL/RANK (data not shown). However, sensorgrams with RANKL, pre-incubated or not with OS-EPS, immobilized on the surface of a CM5 sensor chip revealed different binding response units for RANK (Fig. 5B). To determine the biophysical binding parameters for the ternary complex interactions, real-time SPR spectroscopy was performed (Fig. 6). Surprisingly, the kinetic study showed a significant increase in the association rate of RANK to RANKL pre-incubated with OS-EPS facilitating the complex formation. RANK had a higher affinity for RANKL pre-incubated with OS-EPS surface sensor chips than for RANKL surface sensor chips (> 2-fold). This result would be in favour of an increase in bone resorption which was not observed during the study of osteoclastogenesis (Fig. 4).

RANKL is not only a ligand for RANK but also acts as a ligand for the decoy receptor OPG. To determine whether or not OS-EPS could affect the OPG/RANKL complex, RANKL was immobilized on a sensor chip, and the capacity of OS-EPS to bind to complex OPG/RANKL was analyzed. As with the RANKL/RANK complex, OS-EPS was able to bind to a preformed OPG–RANKL complex (Fig. 5D and 5E), forming another ternary complex, OS-EPS/RANKL/OPG. Also, the pre-incubation of OS-EPS (30 min at room temperature) with OPG or RANKL did not inhibit the capacity of OS-EPS to further bind to the preformed ternary complex OS-EPS/RANKL/OPG (data not shown). However, no modification was observed in the kinetic parameters for the interaction of OPG with RANKL pre-incubated with OS-EPS.

2.5. OS-EPS increases the collagenolytic activity of cathepsin K at physiological plasma pH

Cathepsin K is abundantly and predominantly expressed in osteoclasts and is considered to be the principal protease responsible for the degradation of most of the bone matrix. Cathepsin K can cleave most extracellular substrates, including the collagen triple helix and it has been reported that the collagenolytic activity of cathepsin K at acidic pH depends on a complex formation with chondroitin sulphate, which increases the activity and stability of the enzyme (Li *et al.*, 2002). Recently, Novinec *et al.* (2010) showed that heparin also increased the collagenolytic activity of the enzyme at physiological plasma pH. Therefore we also examined the activity of cathepsin K on collagen in the presence of OS-EPS. Collagenolytic assays (Fig. 7) show that cathepsin K is capable of digesting type I collagen on its own. Heparin and OS-EPS increased the collagenolytic activity of cathepsin K, whereas chondroitin sulphate and dermatan sulphate decreased the extent of collagen digestion.

2.6. OS-EPS induces trabecular bone loss.

During the 28 days of this study all the mice from the different treatment groups (OS-EPS, EPS and heparin-treated) gained weight. No significant differences with respect to weight gain were found between those mice treated with either OS-EPS or EPS or heparin or age-matched controls. However, at the femur level, micro-CT scanner analysis revealed that the mouse femur was characterized by major remodelling activities when compared to the control femurs (Fig.8A). OS-EPS thus resulted in a reduction in cancellous bone volume when compared with controls. The effect of OS-EPS on cancellous bone was similar to that of our positive control (heparin). OS-EPS did not modify cortical bone volume (data not shown) but significantly reduced trabecular bone volume ($p < 0.01$; Fig.8A). The trabecular number (Tb.N) was significantly reduced by OS-EPS ($p < 0.05$), whereas the trabecular space (Tb.Sp) increased ($p < 0.05$). Trabecular thickness (Tb.Th) was not significantly altered (Fig. 8). However, no significant difference in cancellous bone volume (BV/TV) was found between EPS-treated mice and age-matched control mice, highlighting the importance of sulphation in trabecular bone loss.

Histologic sections were stained with TRAP or ALP to quantify osteoclast or osteoblast surface-based data, respectively. Figure 8B shows that the osteoblast surface parameter was not significantly different when comparing OS-EPS or EPS-treated mice and age-matched controls. In contrast, OS-EPS produced an increase in the percentage of cancellous bone covered by osteoclasts.

Whereas mice given 6 mg/kg of OS-EPS showed a 125% \pm 23% ($p < 0.05$) increase in osteoclast surface, the osteoclast surface was unaffected by treatment with EPS (Fig. 8B).

3. Discussion

In the present study, we have shown that long-term administration of OS-EPS, a 'heparin-like' component (with uronic acid and sulphate content comparable to that of heparin) with 'heparin-like' activity (anticoagulant properties), causes cancellous bone loss in mice due, in part, to an increase in the number of osteoclasts lining the trabecular bone surface. Our results are therefore similar to results published many years ago, in which long-term administration of heparin was shown to lead to the development of osteoporosis (Muir *et al.*, 1996). Similarly, Barbour *et al.* (1994) showed that 36% of pregnant women undergoing long-term heparin treatment had a 10% reduction in femoral bone mineral density. Both heparin (Muir *et al.*, 1996; Muir *et al.*, 1997, Rajgopal *et al.*, 2008) and OS-EPS increase the process of bone resorption. Although heparin and OS-EPS have similar effects on osteoclast numbers, heparin was found to decrease osteoblast numbers (Muir *et al.*, 1996; Muir *et al.*, 1997, Rajgopal *et al.*, 2008), whereas OS-EPS has no effect. These effects resulting in bone loss begin early in the course of OS-EPS treatment (data not shown). However, the mechanism sustaining osteoporosis was unclear and it was difficult to determine whether these effects on bone resorption were due to the direct effect of OS-EPS on osteoclasts or indirectly *via* its osteoblast activity.

GAGs exhibit several kinds of biological activities by binding to various extracellular molecules and play a pivotal role in bone metabolism. Indirect proof of heparan sulphate proteoglycan (HSPG) involvement in osteoclast function was described in a publication that demonstrated that heparanase, a HS-degrading endoglycosidase expressed in osteoblastic cells, stimulates bone formation and bone mass (Kram *et al.*, 2006). The effect of GAGs on osteoclastogenesis is controversial. For example, Ariyoshi *et al.* (2008) and Shinmyozu *et al.* (2007) showed inhibition of osteoclastogenesis after direct interaction between GAGs and RANKL. On the contrary, Irie *et al.* (2007) showed that osteoclastic bone resorption was stimulated by inhibiting OPG activity. Our results clearly demonstrated that OS-EPS inhibited osteoclastogenesis in the two systems tested. Furthermore, we demonstrated the importance of the sulphation of the exopolysaccharide in their inhibitory effect. Sulphation also plays a key role in the biological activities of GAGs, as revealed by the present work. Sulphated polysaccharides enhance the biological activity of both the homodimers and heterodimers in bone morphogenetic protein (BMP) by continuously serving the ligands to their signalling receptors expressed on cell membranes, similar to oversulphated chondroitin sulphate which binds to BMP-4 and enhances osteoblast differentiation (Miyazaki *et al.*, 2008). In addition, Kumarasuriyar *et al.* (2009) showed that the chlorate-induced-desulphation of GAGs expressed by MG63 cells delayed *in vitro* osteogenesis.

As our *in vitro* data are in favour of OS-EPS having direct inhibitory activity on osteoclastogenesis, we analyzed the effects of OS-EPS on the adhesion of osteoclast precursors, demonstrating a sequential effect of OS-EPS on RANKL-induced osteoclastogenesis. OS-EPS inhibits the early stage of osteoclast precursor adhesion and consequently inhibits the cell fusion stage. The alteration in cell adhesion and morphology prevents the cell fusion of osteoclast precursors and blocks osteoclast resorption which is particularly sensitive to cell morphology to develop their brush border (Rousselle and Heymann, 2002). However, the question remains of how we can explain the major discrepancies between the *in vivo* and *in vitro* results.

In this context, we first analyzed the interaction of OS-EPS with the OPG/RANK/RANKL molecular triad and the effect of OS-EPS on adhesion of osteoclast precursors. OPG contains a heparin-binding domain and, like heparin (K_D : 0.28 nM; Theoleyre *et al.*, 2006), strongly binds to OS-EPS (K_D : 0.22 nM). The sulphation is essential as a totally desulphated heparin loses its capacity to bind OPG. Here, we clearly showed that OS-EPS can form a hetero-molecular complex (OS-EPS/RANKL/RANK or OS-EPS/RANKL/OPG), as demonstrated using the surface plasmon resonance technique, and that RANK had a higher affinity for RANKL pre-incubated with OS-EPS than for RANKL alone. On the contrary, OS-EPS did not interfere in the binding of RANKL by OPG. These results also revealed that RANKL had higher affinity for OS-EPS ($K_D = 91$ pM) than for OPG ($K_D = 0.27$ nM, Kwan Tat *et al.*, 2006). In conclusion, the preferential binding of RANKL to OS-EPS made it easier for the binary OS-EPS/RANKL complex to form, which, in turn, may facilitate ternary OS-EPS/RANKL/RANK complex formation, which would be in favour of an increase in bone resorption. Secondly, we analyzed the collagenolytic activity of cathepsin K at pH 7.40. Like heparin, OS-EPS increased the collagenolytic activity of cathepsin K. This shows that the molecular mechanism behind

the unique collagenolytic activity of cathepsin K depends on the environment and suggests that it may also be an important factor in cathepsin K regulation *in vivo*. Given that cathepsin K is one of the major factors playing a part in osteoporosis (Stoch *et al.*, 2008), it seems a plausible target for orally administered exopolysaccharides, which would be also in favour of an increase in bone resorption.

The effect observed *in vivo* may be also explained by its effects on the bone osteoblast compartment and then by the dysregulation of the balance between osteoblasts and osteoclasts or by a slow-down in bone remodeling. Osteoblastic cells produce a complex extracellular matrix composed of a mixture of PGs, collagens and non-collagenous proteins. The interaction of PGs with matrix effector macromolecules via either their GAG chains or their protein core is critical in regulating a variety of cellular events. Alterations in the structural composition of the GAG/PG components of the extracellular matrix may have important consequences on cell proliferation and/or differentiation. Recently, Haupt *et al.* (2009) demonstrated the dependence of osteogenesis on specific HS chains, in particular those associated with glypican-3. The differentiating osteoblast-committed cells produced a homogenous HS species (21 kDa), which correlated with an increase in HSPG glypican-3. Abrogation of glypican-3 reduced expression of the osteogenic transcription factor Runx2. The data demonstrated close links between HS modifications and progression of osteogenic precursors through their developmental program.

Our results showed that (1) OS-EPS reduced expression of ALP, coll α I, and Runx2 (preosteoblast stage) in BMSC cells, and enhanced OC and BSP (mature osteoblast stage); (2) OS-EPS did not modulate expression of RANKL by mature osteoblasts; (3) exogenous application of OS-EPS to cultures of primary BMSCs during *in vitro* differentiation completely blocked BMSC mineralization; (4) OS-EPS strongly reduced the proliferation of differentiating osteoblast BMSC cells. This inhibition of proliferation was not due to the induction of apoptosis. These results suggest that OS-EPS reduces proliferation and accelerates osteoblastic differentiation, leading to strong inhibition of mineralized nodule formation which would be in favour of an increase in bone resorption. However, no significant difference in osteoblast surface was found between OS-EPS-treated mice and age-matched control mice. Although the explanation for these conflicting results is unclear, the findings in a whole bone organ culture system are more likely to reflect events *in vivo* than those that occur in isolated osteoblast cultures. It is possible that this reflects the propensity of OS-EPS to bind to other critical growth factors, such as FGF, BMP and tumor growth factor β 1 (TGF β 1).

FGF control the proliferation and differentiation of osteoblast cells (Xiao *et al.*, 2010). FGF2 is thus a powerful promoter of bone growth, enhancing mineralized nodule formation (Downey *et al.*, 2009). This effect is mediated via HSPGs that coordinate the interaction of FGFs with their high-affinity tyrosine kinase receptors, the FGFRs (Eswarakumar *et al.*, 2005). The interaction of PGs with FGFs provides a physiological mechanism for regulation of FGF signalling, FGFR1, and the extracellular signal-regulated kinase pathway. Furthermore, osteoclast differentiation and activity are regulated by GAGs at different levels, as revealed in previous studies. FGF-2 induces, after binding to HS, the expression of RANKL and osteoclast maturation by rheumatoid synovial fibroblasts. FGF-2 not only increases the proliferation of rheumatoid synovial fibroblasts, but is also involved in osteoclast maturation, which leads to bone destruction in rheumatoid arthritis (Nakano *et al.*, 2004). Matou *et al.* (2005) showed the binding of OS-EPS to FGF-2, therefore we hypothesize that FGF-2 can induce bone resorption after binding to OS-EPS. HS and chondroitin sulphate directly regulate the BMP-mediated differentiation of mesenchymal stem cells (hMSCs) into osteoblasts. BMPs, which have been shown to be heparin-binding proteins, induce osteoblast differentiation in hMSCs (Manton *et al.*, 2007). The role of heparin in the biological activity of BMP remains unclear. Heparin inhibits the binding of BMP-2 to BMPR and subsequent mRNA expression of Runx2, as well as phosphorylation of Smad and MAPK signal transduction. Furthermore, heparin has been found to suppress the differentiation of osteoblastic MC3T3-E1 cells treated with BMP-2 (Kanzaki *et al.*, 2008). In contrast, Zhao *et al.* (2006) showed that heparin enhanced BMP-induced osteoblast differentiation by protecting BMPs from degradation and inhibition by BMP antagonists. TGF β 1 is a known inhibitor of osteoprogenitor growth, which has a higher affinity than several other bone-related, heparin-binding growth factors (Manton *et al.*, 2006). This binding suggests that GAGs play a critical role in regulating TGF- β availability. Overcoming such sugar-mediated inhibition may prove important for wound repair.

Given the importance of oversulphated exopolysaccharides for bone metabolism, it can be anticipated that OS-EPS, thanks to its structural similarity with HS chains, somehow interferes with the biological activities of these cell surface- and extracellular matrix-associated molecules. Taken together, these data show different levels of bone resorption regulation by GAGs or exopolysaccharides, most of them leading to proresorptive effects.

4. Materials and methods

Materials. Human M-CSF, human RANK and human OPG were obtained from R&D Systems (Abington, UK). Human RANKL was kindly provided by Amgen Inc. (Thousand Oaks, USA). Heparin sodium salt, heparan sulphate from bovine kidney, heparan sulphate from porcine intestinal mucosa, chondroitin sulphate from shark cartilage, dermatan sulphate from porcine intestinal mucosa and hyaluronic acid were purchased from Sigma (St Quentin Fallavier, France). The two low molecular weight exopolysaccharides (EPS and OS-EPS) were obtained from high molecular weight exopolysaccharide (GY 785). The isolation procedure and characteristics of the GY 785 *Alteromonas infernus* strain have been reported previously [Ragueneas *et al.*, 1997]. The GY 785 was produced, purified and characterized as previously described [Guezennec *et al.*, 1998]. The preparation of EPS and OS-EPS derivatives was performed as previously described. Briefly, GY 785 was first depolymerized by a process using a modification of the procedure of Nardella *et al.* (1996). Four hundred milligrams GY 785 were dissolved in water (95 ml) in a reaction vessel, and 5 ml of 3×10^{-3} M cupric acetate monohydrate were added. The temperature was kept at 60°C. A 0.07% (w/w) hydrogen peroxide solution was then added at a flow rate of 60 ml/h. The reaction was stopped after 2.5 h, and the contaminating copper ions were removed from the product by chromatography on Chelex 20 resin (in Na. form), with water as the eluent. The solution was concentrated, desalinated by ultrafiltration with a 1000 Da cut-off membrane and then freeze-dried. EPS was chemically oversulphated according to a previously described direct sulphation procedure (Nishino *et al.* 1992). After sulphation, OS-EPS with a 40% sulphate group (w/w) was obtained.

The purities of the final products (EPS and OS-EPS) were estimated at > 80%, as judged by the use of well-described chemical methods (Colliec-Jouault *et al.*, 2001): monosaccharidic content was determined by GC analysis of trimethylsilyl derivatives after acidic methanolysis; protein content was determined by Pierce BCA Protein Assay Reagent; nitrogen, hydrogen, carbon and sulphur contents were determined by elemental analysis by the Central Microanalysis Department of the CNRS (Gif/Yvette, France). Sulphate content (sodium salt) was deduced from sulphur analysis according to the following relation: sulphate group % = $3.22 \times S$ %. Sulphate content was also determined by Fourier transform infrared analysis. Pellets were obtained by careful grinding of a mixture of 2 mg of EPS with 200 mg of dry KBr. Infrared spectra were recorded on a BOMEM M100 Fourier Transform Infrared Spectrometer with resolution of 4 cm^{-1} . EPS and OS-EPS are hygroscopic so in their dry state they may contain between 10 and 20 wt % of water.

Culture medium and preparation of BMSCs. BMSCs were isolated from the bone marrow of 4 week-old Sprague-Dawley rats (Janvier, Le Genest Saint Isle, France). After anesthetization and cervical dislocation, femurs and tibiae were dissected aseptically and cleaned of soft tissues. The BMSCs were then flushed out with a syringe fitted with a 22-gauge needle containing maintenance media (MM) consisting of α -Minimal Essential Medium (α -MEM, Invitrogen) supplemented with 10% fetal bovine serum (FBS) and 1% antibiotics (100 U/mL penicillin and 100 mg/L streptomycin). After centrifugation (5 minutes at 1600 rpm) the cells were resuspended in 20 mL of MM. For osteogenic media (OM) culture conditions, this medium was supplemented with 50 $\mu\text{g}/\text{mL}$ of ascorbic acid (Sigma) and 10^{-8} M dexamethasone (Sigma). Cells between passages 0 and 3 were used for all experiments. The cells were maintained at 37°C in a humidified atmosphere containing 5% CO_2 .

Proliferation of BMSCs. Cells were plated (5×10^4 /well) into a 6-well plate in MM overnight. Then the MM was replaced by fresh OM in the presence or absence of 25 $\mu\text{g}/\text{mL}$ EPS or OS-EPS, and the cells were left to recover for 7 days (the medium was changed every 3 days). Then, the cells in each well were washed three times in 1x Dulbecco phosphate-buffered saline (DPBS), trypsinized and counted in triplicate at days 3 and 7 using blue trypan exclusion dye.

Induction of apoptosis. Programmed cell death was monitored microscopically following Hoechst staining. BMSCs were seeded at 10^4 cells/well in a 24-well plate and cultured for 24 h in MM. Then the MM was replaced with fresh OM in the presence of 25 $\mu\text{g}/\text{mL}$ OS-EPS for 24, 48, and 72 h or 100 nM staurosporine (Sigma) for 16 h as a positive control. At the end of the culture period, the cells were stained with 10 $\mu\text{g}/\text{mL}$ Hoechst reagent for 30 min at 37°C, and then observed under UV microscopy (DMRXA; Leica, Wetzlar, Germany).

Induction of apoptosis was also investigated by cleavage of caspase-3 substrates in supernatants of cultures with or without OS-EPS treatment. BMSCs were seeded at 15×10^3 cells/well (in a 24-well plate), then incubated with OS-EPS (25 $\mu\text{g}/\text{mL}$) for 24, 48, and 72 h. Cells incubated with 1 μM staurosporine for 6 h were used as positive controls. At the end of the incubation period, the cells were

lysed with 50 μ l of RIPA buffer for 30 min. The cells were then scraped off and protein content was quantified in parallel samples using the BCA (bicinchoninic acid + Copper II sulphate) assay. Caspase-3 activity was assessed in 10 μ l of the cell lysate with the CaspACEi Assay System kit (Fluorometric, Promega, Madison, USA) following the manufacturer's instructions.

Time-lapse microscopy. The BMSCs were plated (2×10^3 cells/well) in triplicate into a 24-well plate in MM overnight. Then MM was replaced with fresh OM in the presence or absence of 25 μ g/mL of EPS or OS-EPS. Immediately post-treatment, the cultured dishes were placed on to a time-lapse instrument (Leica) designed to capture transmission-phase images every 10 min from multi-well plates. Images were taken and edited using the MetamorphTM software. Cell divisions were then scored manually.

Cell cycle analysis. Cells were plated in triplicate (2×10^5 /well) in a 6-well plate in MM overnight. Then MM was replaced with fresh OM in the presence or absence of 25 μ g/mL of EPS or OS-EPS. After 48 h the cells were trypsinized and centrifuged at 1600 rpm for 3 min. Cell pellets were fixed in 70% ice-cold ethanol for 30 min and then washed twice in 100 μ l of DPBS. The cells were incubated in phosphate-citrate buffer at room temperature for 30 min then in DPBS containing 0.12% Triton X-100, 0.12 mM EDTA and 100 μ g/ml ribonuclease A at 37°C for 30 min. The cells were then centrifuged, washed twice and incubated in 50 μ g/ml propidium iodide for 20 min at 4°C. Cell cycle distribution was analyzed by flow cytometry F500 (Beckman Coulter France) based on 2N and 4N DNA content using the MultiCycle software.

Mineralization assay. The BMSCs were plated (3.5×10^6 cells/well) in duplicate in a 24-multi-well plate in MM. After 24 hours of culture, the supernatant (MM) containing the non-adherent hematopoietic cells was removed. At confluence (72 h later), the MM was replaced by OM (the medium was changed twice a week) in the presence of 25 μ g/mL of EPS or OS-EPS. After 1 week of culture, the OM was supplemented with 10 mM β -glycerophosphate (Sigma) for 2 weeks (the medium was changed twice a week) in the presence or absence of 25 μ g/ml of EPS or OS-EPS added at different times during the culture period. Then, Alizarin red staining (Alfa Aesar) was used to detect the mineralized nodules formed *in vitro*. The cells were washed in DPBS and fixed in 70% ice-cold ethanol for 1 h. The ethanol was then removed, and the fixed cells were washed three times with distilled water and incubated with alizarin red (40 mM, pH 7.4) for 10 minutes at room temperature. After staining, excessive dye was washed out gently with running water. Calcification deposits typically stained red. All experiments were performed three times.

Osteogenic differentiation assay. The BMSCs were plated (15×10^6 cells/well) in a 6-multi-well plate in MM. After 24 hours of culture, the supernatant (MM) containing the non-adherent hematopoietic cells was removed. At confluence (72 h later), the MM was replaced by OM in the presence of 25 μ g/mL of EPS or OS-EPS (the medium was changed twice a week). After 1 week of culture, the OM was supplemented with 10 mM β -glycerophosphate for 2 weeks (the medium was changed twice a week).

RT-qPCR analysis: Total RNA was isolated from osteogenic cultures at different times using the NucleoSpin II kit (Macherey-Nagel). RNA (500 ng) was reversed-transcribed (RT) using the ThermoSript System (Invitrogen). cDNA synthesis was performed using total RNA with oligo(dT) at 50°C for 1 h. qPCR was performed in triplicate for each sample using 5 μ l 2x SYBR Green Supermix buffer (Bio-Rad, Marnes la Coquette, France), 1 μ l cDNA, 300 nM of each primer, and DEPC H₂O to a final volume of 10 μ l. After denaturing the cDNA at 98°C for 30 sec, amplification and fluorescence determination were carried out in two steps: denaturation at 95°C for 15 sec, and annealing and extension at 60°C for 30 sec. The detection of SYBR Green was during the annealing process. The sequence of the primers used in the PCR reactions is shown in Table 1. Cyc1 cDNA as internal controls were used to normalize the data to determine the relative expression of the target genes. Polymerase chain reactions were carried out in 96-well plates using the Chromo4 System (Bio-Rad).

Collagen digestion: Soluble calf-skin collagen was diluted in 50 mM Hepes, pH 7.40, containing 1 mM EDTA to a final concentration of 0.5 mg/ml. The solutions were supplemented with 2.5 mM DTT and 0.2 mM GAGs and digestion started by addition of cathepsin K (final concentration 0.25 μ M). All reactions were incubated for 12 h at 25°C and then stopped by addition of SDS/PAGE sample buffer. Polypeptides were separated by SDS/PAGE (8%gels) and stained with Coomassie Brilliant Blue R-250.

Differentiation of human CD14⁺ cells into osteoclasts. Human peripheral blood mononuclear cells (PBMCs) were isolated by centrifugation over Ficoll gradient (Sigma Chemicals Co., St. Louis, MO). CD14⁺ cells were magnetically labelled with CD14 Microbeads and positively selected by MACS technology (Miltenyi Biotec, Bergisch Gladbach, Germany). CD14⁺ cells were plated (45×10^3 cells/well) in triplicate in a 96-well plate in α -MEM containing 10% FBS and 25 ng/ml human M-CSF. After 3 days of culture, the medium was replaced with fresh medium containing 10% FBS, 25 ng/ml human M-CSF, with or without 100 ng/ml hRANKL. Then the medium was changed every 4 days. The formation of osteoclasts occurred at around 14 days and was observed by tartrate-resistant acid phosphatase (TRAP) staining. In this experiment, EPS or OS-EPS were added at different times during the culture period. Then, the multinucleated cells (>3 nuclei) were counted under a light microscope (Leica DM IRB, Nanterre, France; Camera: Olympus D70, Analysis software: Olympus DP Controller/Manager, Hamburg, Germany) after TRAP staining (Sigma, Saint Quentin-Fallavier, France)

Differentiation from the murine RAW 264.7 monocytic cell line. Murine RAW 264.7 monocytic cells (ATCC, Promochem, Molsheim, France) were cultured in phenol red-free α -Minimal Essential Medium (α -MEM) (Invitrogen, Eragny, France) supplemented with 10% FBS (Perbio, Logan, USA) and 1% non essential amino acids (Invitrogen). To induce osteoclast formation, RAW 264.7 cells were scraped then incubated at 37°C for 2 minutes to allow adherence of the more differentiated cells. Non-adherent cells were then seeded in fresh medium at a density of 3×10^3 cells/well in a 96-well plate. After 2 hours of culture, the medium was changed for fresh medium containing 100 ng/ml hRANKL with or without 0.5 μ g/ml EPS or OS-EPS. The cells were stained histochemically for TRAP and the number of TRAP-positive multinuclear cells (MNCs) containing 3 or more nuclei was counted.

Adherence of human CD14⁺ cells. Cells were plated (25×10^4 cells/well) in triplicate in a 96-well plate in α -MEM containing 10% FBS and 25 ng/ml human M-CSF for 3 days (time required for these cells to adhere). The medium was then replaced with fresh medium containing α -MEM, 10% FBS and 25 ng/ml human M-CSF in the presence of 1 μ g/ml EPS or OS-EPS for 5 days (the medium was changed once). Then, non-adherent cells in the supernatant were counted in triplicate using blue trypan exclusion dye. The adherent cells were washed three times in DPBS, trypsinized and counted as above.

Surface plasmon resonance-binding assays. Experiments were carried out on a BIAcore 3000 instrument (BIAcore). RANKL, OPG (5 μ g/ml in 10 mM acetate buffer, pH 4.0 and pH 5.0 (1:1;v/v)) and RANK (10 μ g/ml in 10 mM acetate buffer, pH 5.0) were covalently immobilized to the dextran matrix of a CM5 sensor chip (BIAcore) via its primary amino groups at a flow rate of 30 μ l/min. Immobilization levels ranging between 4000 resonance units (RU) (RANKL and OPG) and 5000 RU (RANK) were obtained. EPS and OS-EPS K_D values for OPG, RANK and RANKL were determined using single cycle kinetics, starting with 1 nM OS-EPS or 100nM EPS (OPG), 250 nM OS-EPS or 2 μ M EPS (RANKL) and 100 nM OS-EPS or 2 μ M EPS (RANKL), then 1/2 dilutions. For binding analysis over the immobilized RANKL, OPG or RANK chip, the concentrations of 1 μ g/ml OPG, 2 μ g/ml RANK, 0.5 μ g/ml RANKL, 20 μ M GAGs (heparin, or heparan sulphate, or chondroitin sulphate, or dermatan sulphate, or hyaluronic acid), 20 μ M EPS and 200 nM OS-EPS were used. Binding assays were performed at 25°C in 10 mM Hepes buffer, pH 7.4, containing 0.15 M NaCl and 0.005% P20 surfactant (HBS-P buffer, BIAcore) at a flow rate of 30 μ l/min. Control sensorgrams (flow cell without RANKL, OPG and RANK) were automatically subtracted from the sensorgrams obtained with immobilized RANKL or OPG or RANK to yield true binding responses. The resulting sensorgrams were fitted using BiaEval 4.1 software (BIAcore).

Animal studies. Twenty-four 4-week-old male C3H/HeN mice (Janvier, Le Genest Saint Isle, France) were housed in pathogen-free conditions at the Experimental Therapy Unit (Nantes Faculty of Medicine, France) in accordance with the institutional guidelines by the French Ethical Committee and under the supervision of authorized investigators. After 7 days of acclimatization the animals were assigned randomly to four groups: control (CT), heparin (Sigma H4784, 140U/mg, 50mg/ml), EPS and OS-EPS. All mice received a (6 mg/kg) daily s.c. injection for a period of 28 days, consistent with the period of rapid growth in young mice. On the 29th day, the animals were anesthetized with isoflurane (0.2% air, delivered via nosecone) and sacrificed by cervical dislocation. Bilateral femurs from each animal were dissected for histological studies and micro-architectural parameter quantification. Two independent experiments were performed.

Histological analysis. After sacrifice, the left femurs were cleaned from adjacent tissues and fixed in 10% buffered formaldehyde. Then samples were decalcified in 4% EDTA 0.2% paraformaldehyde (pH 7.4) buffer for 4 weeks and embedded in paraffin wax for TRAP and ALP staining. Five- μ m-thick sections were cut through the femur (microtome: Leica SM 2500; Leica Instruments GmbH) and mounted on glass slides. Analysis and quantification of osteoblastic and osteoclastic areas were done using a Leica Q500 image analysis system.

Micro-computed tomography (μ CT). After sacrifice, the right femur from each animal was dissected from the soft tissues, fixed in 10% buffered formaldehyde and the distal metaphysis was used for micro-computed tomography (μ -CT) on a SkyScan-1072 (SkyScan, Aartselaar, Belgium). CT-Analyser software (from SkyScan) was used to analyse the structure of the sample, using the global segmentation method. Two-dimensional (2D) images were used to generate three-dimensional (3D) reconstructions and to calculate morphometric parameters with the SkyScan CtAn 3D creator software supplied with the instrument. Analysis was performed for the trabecular bone, whereby the trabecular region was precisely contoured in each single cross section manually. Bone volume ratio (BV/TV), trabecular thickness (Tb.Th), trabecular number (Tb.N) and trabecular space (Tb.Sp) were assessed.

Statistical analysis. All analyses were performed using GraphPad InStat v3.02 software (La Jolla, CA). The mean \pm SD was calculated for all conditions and compared by ANOVA. *In vivo* experimentation results were analyzed with the unpaired nonparametric Mann–Whitney U test using two-tailed P-values. Differences relative to a probability of two-tailed $p < 0.05$ were considered significant.

Acknowledgments

This work was supported by the Région des Pays de la Loire [Program entitled “Ciblage Moléculaire et Applications Thérapeutique” (CIMATH)] and by the ANR 2007 INSERM Pathophysiology of Human Diseases project N° R07196NS. Carmen RUIZ VELASCO received a fellowship from the Région des Pays de la Loire. We thank Régis Brion and Pierre Veigel (ESBS) for their technical assistance in preparing mature osteoclasts isolated from the cultures of CD14⁺ cells and determining collagenolytic activity. We thank Verena STRESING for proof reading and helpful discussions.

Abbreviations

GAG: glycosaminoglycan
PG: proteoglycan
OPG: osteoprotegerin
RANK: receptor Activator of NF- κ B
RANKL: RANK Ligand
HS: heparan sulphate
EPS: exopolysaccharide
OS-EPS: oversulphated EPS
FGF: fibroblast growth factor
VEGF: vascular endothelial growth factor
BMSC: bone marrow stem cell
ALP: alkaline phosphatase
Coll α 1: type 1 collagen
BSP: bone sialoprotein
OC: osteocalcin
SPR: surface plasmon resonance
BMP: bone morphometric protein
TGF β : tumour growth factor β

5. References

- Ariyoshi W, Takahashi T, Kanno T, Ichimiya H, Shinmyouzu K, Takano H, Koseki T, Nishihara T. 2008. Heparin inhibits osteoclastic differentiation and function. *J. Cell. Biochem.* 103: 1707-1717.
- Barbour LA, Kick SD, Steiner JF, LoVerde ME, Heddleston LN, Lear JL, Baron AE, Barton PL. 1994. A prospective study of heparin-induced osteoporosis in pregnancy using bone densitometry. *Am. J. Obstet. Gynecol.* 170 : 862-869.
- Bernas GC. 2003. Angiotherapeutics from natural products: from bench to clinics? *Clin Hemorheol Microcirc.* 29: 199-203.
- Bernfield M, Gotte M, Park PW, Reizes O, Fitzgerald ML, Lincecum J, Zako M. 1999. Functions of cell surface heparan sulphate proteoglycans. *Annu. Rev. Biochem.* 68:729-777.
- Collic-Jouault S, Chevotot L, Helley D, Ratiskol J, Bros A, Siquin C, Roger O and Fischer AM. 2001. Characterization, chemical modifications and in vitro anticoagulant properties of an exopolysaccharide produced by *Alteromonas infernus*. *Biochim Biophys Acta.* 1528: 141–151.
- Downey ME, Holliday LS, Aguirre JI, Wronski TJ. 2009. In vitro and in vivo evidence for stimulation of bone resorption by an EP4 receptor agonist and basic fibroblast growth factor: Implications for their efficacy as bone anabolic agents. *Bone.* 44: 266-274.
- Eswarakumar VP, Lax I, Schlessinger J. 2005. Cellular signaling by fibroblast growth factor receptors. *Cytokine GrowthFactor Rev.* 16: 139–149.
- Franz, G and Alban S. 1995. Structure-activity relationship of antithrombotic polysaccharide derivatives. *Int. J. Biol. Macromol.* 17: 311-314.
- Guezennec JG, Pignet P, Lijour Y, Gentric E, Ratiskol J, Collic-Jouault S. 1998. Sulphation and depolymerization of a bacterial exopolysaccharide from hydrothermal origin. *Carbohydr Polymers.* 37: 19–24.
- Guezennec J. 2002. Deep-sea hydrothermal vents: a new source of innovative bacterial exopolysaccharides of biotechnological interest? *J Ind Microbiol Biotechnol.* 29: 204–208.
- Haupt LM, Murali S, Mun FK, Teplyuk N, Mei LF, Stein GS, van Wijnen AJ, Nurcombe V, Cool SM. 2009. The heparan sulphate proteoglycan (HSPG) glypican-3 mediates commitment of MC3T3-E1 cells toward osteogenesis. *J Cell Physiol.* 220: 780-791.
- Irie A, Takami M, Kubo H, Sekino-Suzuki N, Kasahara, K, Sanai Y. 2007. Heparin enhances osteoclastic bone resorption by inhibiting osteoprotegerin activity. *Bone.* 41: 165- 174.
- Jackson RA, Murali S, van Wijnen AJ, Stein GS, Nurcombe V, Cool SM. 2007. Heparan sulphate regulates the anabolic activity of MC3T3-E1 preosteoblast cells by induction of Runx2. *J Cell Physiol.* 210: 38-50.
- Kanzaki S, Takahashi T, Kanno T, Ariyoshi W, Shinmyouzu K, Tujisawa T, Nishihara T. 2008. Heparin inhibits BMP-2 osteogenic bioactivity by binding to both BMP-2 and BMP receptor. *J Cell Physiol.* 216: 844-850.
- Kong YY, Yoshida H, Sarosi I, Tan HL, Timms E, Capparelli C, Morony S, Oliveira-dos-Santos AJ, Van G, Itie A, *et al.* 1999. OPGL is a key regulator of osteoclastogenesis, lymphocyte development and lymph-node organogenesis. *Nature.* 397: 315-323.
- Kram V, Zcharia E, Yacoby-Zeevi O, Metzger S, Chajek-Shaul T, Gabet Y, Müller R, Vlodavsky I, Bab I. 2006. Heparanase is expressed in osteoblastic cells and stimulates bone formation and bone mass. *J Cell Physiol.* 207: 784-792.

- Kumarasuriyar A, Lee I, Nurcombe V, Cool SM. 2009. De-sulphation of MG-63 cell glycosaminoglycans delays in vitro osteogenesis, up-regulates cholesterol synthesis and disrupts cell cycle and the actin cytoskeleton. *J Cell Physiol.* 219: 572-583.
- Kwan Tat S, Padrines M, Theoleyre S, Heymann D, Fortun Y. 2004. IL-6, RANKL, TNF-alpha/IL-1: interrelations in bone resorption pathophysiology. *Cytokine Growth Factor Rev.* 15: 49-60.
- Kwan Tat S, Padrines M, Théoleyre S, Couillaud-Battaglia S, Heymann D, Redini F, Fortun Y. 2006. OPG/membranous--RANKL complex is internalized via the clathrin pathway before a lysosomal and a proteasomal degradation. *Bone*, 39: 706-715.
- Lamoureux F, Baud'huin M, Duplomb L, Heymann D, Redini F. 2007. Proteoglycans: key partners in bone cell biology. *Bioessays.* 29 : 758-771.
- Lamoureux F, Picarda G, Garrigue-Antar L, Baud'huin M, Trichet V, Vidal A, Miot-Noirault E, Pitard B, Heymann D, Redini F. 2009. Glycosaminoglycans as potential regulators of osteoprotegerin therapeutic activity in osteosarcoma. *Cancer Res.* 69: 526-536.
- Li, Z., Hou WS, Escalante-Torres CR, Gelb BD and Brömme D. 2002. Collagenase activity of cathepsin K depends on complex formation with chondroitin sulfate. *J. Biol. Chem.* 277, 28669-28676.
- Ling L, Dombrowski C, Foong KM, Haupt LM, Stein GS, Nurcombe V, van Wijnen AJ, Cool SM. 2010. Synergism between Wnt3a and heparin enhances osteogenesis via a phosphoinositide 3-kinase/Akt/RUNX2 pathway. *J Biol Chem.* 285: 26233-26244.
- Manton KJ, Sadasivam M, Cool SM, Nurcombe V. 2006. Bone-specific heparan sulphates induce osteoblast growth arrest and downregulation of retinoblastoma protein. *J Cell Physiol.* 209: 219-229.
- Manton KJ, Leong DF, Cool SM, Nurcombe V. 2007. Disruption of heparan and chondroitin sulphate signaling enhances mesenchymal stem cell-derived osteogenic differentiation via bone morphogenetic protein signaling pathways. *Stem Cells.* 25: 2845-2854.
- Marie PJ. 2003. Fibroblast growth factor signaling controlling osteoblast differentiation. *Gene.* 316: 23-32.
- Matou S, Collic-Jouault S, Galy-Fauroux I, Ratiskol J, Siquin C, Guezennec J, Fischer AM, Helley D. 2005. Effect of an oversulphated exopolysaccharide on angiogenesis induced by fibroblast growth factor-2 or vascular endothelial growth factor in vitro. *Biochem Pharmacol.* 69: 751-759.
- Mayer AM, Lehmann VK. 2001. Marine pharmacology in 1999: antitumor and cytotoxic compounds. *Anticancer Res.* 21: 2489-2500.
- Miraoui H, Oudina K, Petite H, Tanimoto Y, Moriyama K, Marie PJ. 2009. Fibroblast growth factor receptor 2 promotes osteogenic differentiation in mesenchymal cells via ERK1/2 and protein kinase C signaling. *J Biol Chem.* 284: 4897-4904.
- Miyazaki T, Miyauchi S, Tawada A, Anada T, Matsuzaka S, Suzuki O. 2008. Oversulphated chondroitin sulphate-E binds to BMP-4 and enhances osteoblast differentiation. *J Cell Physiol.* 217: 769-777.
- Muir JM, Andrew M, Hirsh J, Weitz JI, Young E, Deschamps P, Shaughnessy SG. 1996. Histomorphometric analysis of the effects of standard heparin on trabecular bone in vivo. *Blood.* 88: 1314-1320.
- Muir JM, Hirsh J, Weitz JI, Andrew M, Young E, Shaughnessy SG. 1997. A histomorphometric comparison of the effects of heparin and low-molecular-weight heparin on cancellous bone in rats. *Blood.* 89: 3236-3242.

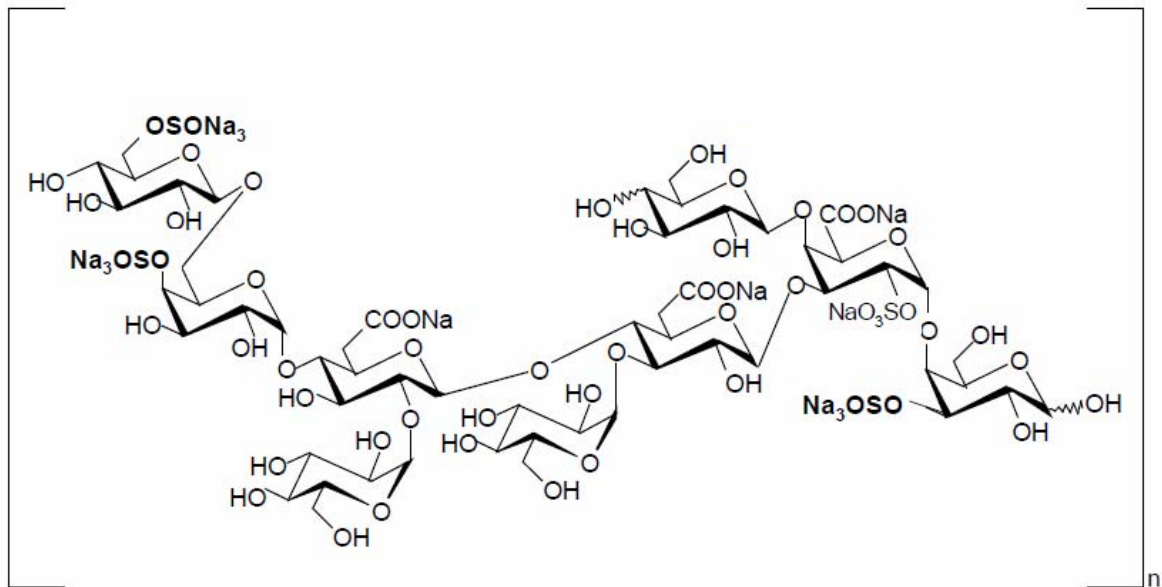
- Nakano, K., Okada, Y., Saito, K., Tanaka, Y., 2004. Induction of RANKL expression and osteoclast maturation by the binding of fibroblast growth factor 2 to heparan sulphate proteoglycan on rheumatoid synovial fibroblasts. *Arthritis Rheum.* 50: 2450-2458.
- Nardella A, Chaubet F, Boisson-Vidal C, Blondin C, Durand P, Jozefonvicz J. 1996. Anticoagulant low molecular weight fucans produced by radical process and ion exchange chromatography of high molecular weight fucans extracted from the brown seaweed *Ascophyllum nodosum*. *Carbohydr Res.* 289: 201-208.
- Nichols CA, Guezennec J, Bowman JP. 2005. Bacterial exopolysaccharides from extreme marine environments with special consideration of the southern ocean, sea ice, and deep-sea hydrothermal vents: a review. *Mar Biotechnol (NY)* 7: 253-271.
- Nishino T, Nagumo T. 1992. Anticoagulant and antithrombin activities of oversulfated fucans. *Carbohydr Res.* 229: 355-362.
- Novinec M, Kovacioc L, Lenarcic B, Baici A. 2010. Conformational flexibility and allosteric regulation of cathepsin K. *Biochem. J.* 429: 379–389.
- Raguénès G, Peres A, Ruimy R, Pignet P, R Christen R, Loaec M, Rougeaux H, Barbier G and Guezennec J. 1997. *Alteromonas infernus* sp.nov, a new polysaccharide producing bacterium isolated from a deep-sea hydrothermal vent. *J. Appl. Bacteriol.* 82: 422-430
- Rajgopal, R., Bear, M., Butcher, M. K., Shaughnessy, S. G., 2008. The effects of heparin and low molecular weight heparins on bone. *Thromb. Res.* 12:, 293-298.
- Roger O, Kervarec N, Ratiskol J, Collic-Jouault S, Chevolut L. 2004. Structural studies of the main exopolysaccharide produced by the deep-sea bacterium *Alteromonas infernus*. *Carbohydr Res.* 229: 2371–2380.
- Rousselle AV, Heymann D. 2002. Osteoclastic acidification pathways during bone resorption. *Bone.* 30: 533-540.
- Ruiz Velasco C., Collic-Jouault S., Redini F, Heymann D., Padrines M. 2010, Proteoglycans on bone tumor development. *Drug Discov. Today.* 15: 553-560.
- Shinmyozu K, Takahashi T, Ariyoshi W, Ichimiya H, Kanzaki S, Nishihara T. 2007. Dermatan sulphate inhibits osteoclast formation by binding to receptor activator of NF-kappa B ligand. *Biochem. Biophys. Res. Commun.* 354: 447-452.
- Simonet WS, Lacey DL, Dunstan CR, Kelley M, Chang MS, Luthy R, Nguyen HQ, Wooden S, Bennett L, Boone T *et al.* 1997. Osteoprotegerin: a novel secreted protein involved in the regulation of bone density. *Cell.* 89: 309-319.
- Standal T, Seidel C, Hjertner O, Plesner T, Sanderson RD, Waage A, Borset M, Sundan A. 2002. Osteoprotegerin is bound, internalized, and degraded by multiple myeloma cells. *Blood.* 100: 3002-3007.
- Stoch, SA and Wagner JA. 2008. Cathepsin K inhibitors: a novel target for osteoporosis therapy. *Clin. Pharmacol. Ther.* 83, 172–176.
- Sutherland IW. 1996. *Biotechnology Second, completely revised edition, vol. 6, Products of primary metabolism*, Rehm H. J. and Reed G. (eds), VCH, Weinheim, pp. 613-657.
- Theoleyre S, Kwan Tat S, Vusio P, Blanchard F, Gallagher J, Ricard-Blum S, Fortun Y, Padrines M, Redini F, Heymann D. 2006. Characterization of osteoprotegerin binding to glycosaminoglycans by surface plasmon resonance: role in the interactions with receptor activator of nuclear factor kappaB ligand (RANKL) and RANK. *Biochem. Biophys. Res. Commun.* 34: 460-467.

Wittrant Y, Théoleyre S, Chipoy C, Padrines M, Blanchard F, Heymann D, Rédini F. 2004. RANKL/RANK/OPG: new therapeutic targets in bone tumours and associated osteolysis. *Biochim Biophys Acta*. 1704: 49-57.

Xiao L, Sobue T, Esliger A, Kronenberg MS, Coffin JD, Doetschman T, Hurley MM., 2010. Disruption of the Fgf2 gene activates the adipogenic and suppresses the osteogenic program in mesenchymal marrow stromal stem cells. *Bone*. 47: 360-370.

Yasuda H, Shima N, Nakagawa N, Mochizuki SI, Yano K, Fujise N, Sato Y, Goto M, Yamaguchi K, Kuriyama M, *et al.* 2004. Identity of osteoclastogenesis inhibitory factor (OCIF) and osteoprotegerin (OPG): a mechanism by which OPG/OCIF inhibits osteoclastogenesis in vitro. *Endocrinology*. 139: 1329-1337.

Zhao B, Katagiri T, Toyoda H, Takada T, Yanai T, Fukuda T, Chung UI, Koike T, Takaoka K, Kamijo R. 2006. Heparin potentiates the in vivo ectopic bone formation induced by bone morphogenetic protein-2. *J Biol Chem*. 281: 23246-23253.



SO₃Na : native EPS

SO₃Na : OS-EPS after O-Sulfatation

Figure 1: Branched nonasaccharidic repetitive unit of native EPS.

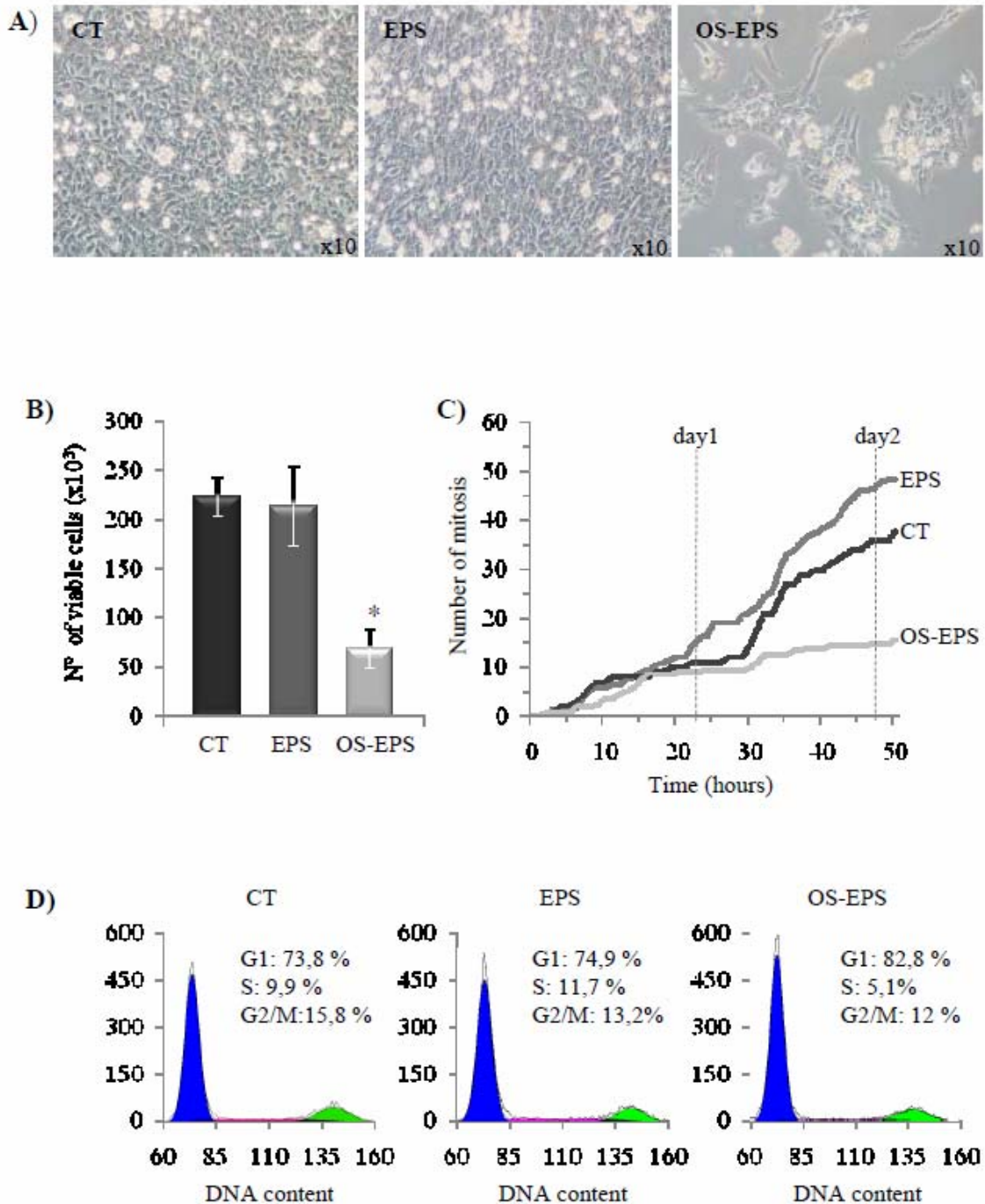


Figure 2: OS-EPS inhibits BMSCs proliferation during osteoblastic differentiation. BMSCs were incubated in osteogenic media in the presence of 25µg/ml of EPS or OS-EPS. After 7 days, images of treated cells were taken under light microscopy (A) and the number of viable cells was determined by trypan blue counting (*: $p < 0.01$) (B). Cumulative mitosis of the first 48h of incubation with EPS or OS-EPS was manually scored from time-lapse analysis (C). Cell cycle distribution of BMSCs incubated with EPS or OS-EPS for 48 h was analyzed by propidium iodide staining and FACS analysis (D).

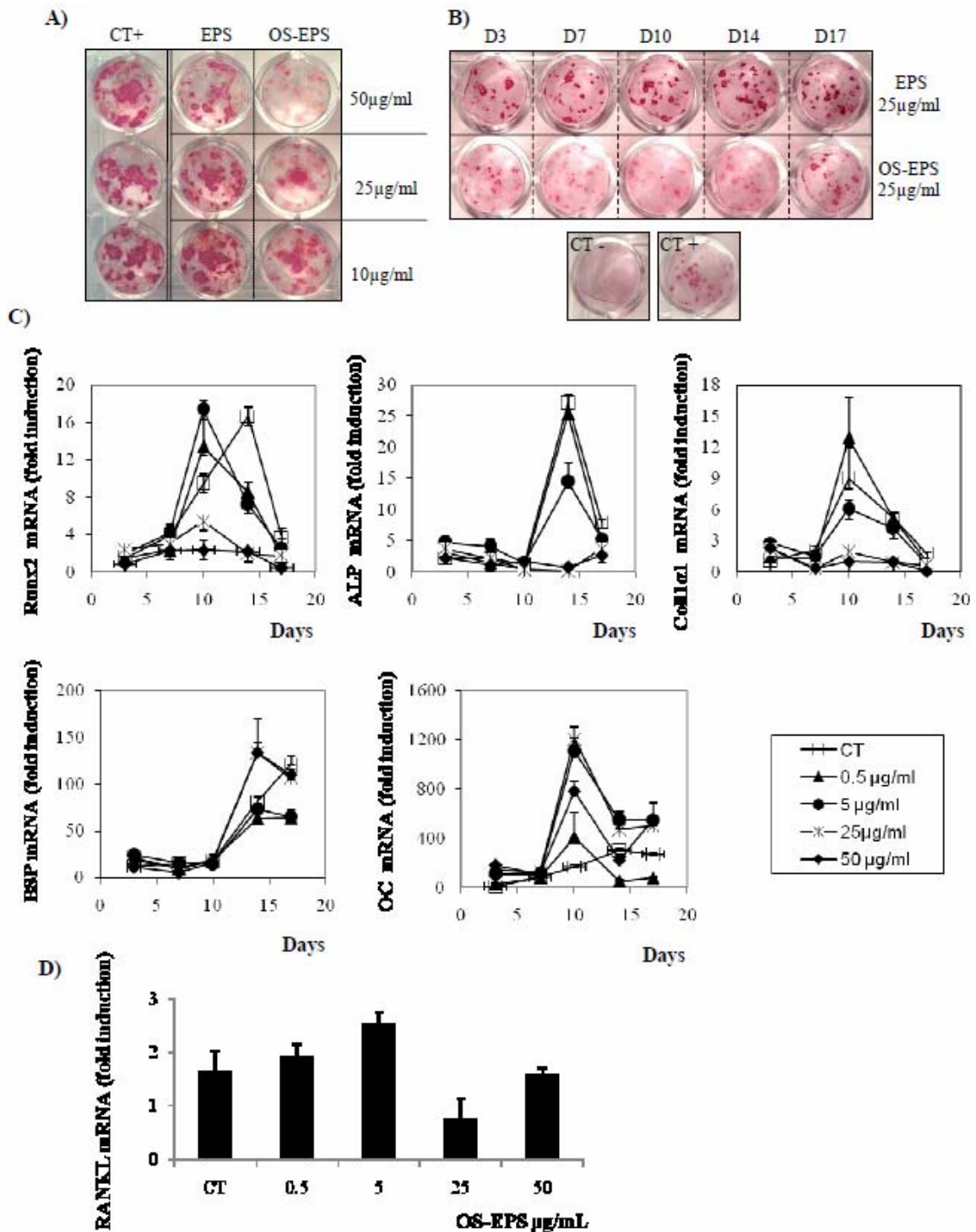


Figure 3: OS-EPS inhibits the extracellular matrix mineralization from BMSCs in a dose-dependent manner. (A) BMSCs were incubated in osteogenic media for three weeks in the presence or absence of increased concentrations of EPS and OS-EPS. (B) EPS or OS-EPS at 25µg/ml were added at different times during the culture period as indicated in the presence of 50 µg/mL ascorbic acid and 10⁻⁸ M dexamethasone. Controls were done in the absence of exopolysaccharide and in the presence (CT+) or absence (CT-) of 50 µg/mL ascorbic acid (Sigma) and 10⁻⁸ M dexamethasone. At the end of the culture period, Alizarin Red staining was used (original magnification x 10). (C) Gene expression profiles of the bone-specific markers for osteoblastic differentiation were determined by qPCR in the absence (CT) or presence of different OS-EPS concentrations. The data show fold differences in expression following normalization against Cyc1. (D) The RANKL expression profile was determined by qPCR in the absence (CT) or presence of different OS-EPS concentrations after 17 days. The data show fold differences in expression following normalization against Cyc1.

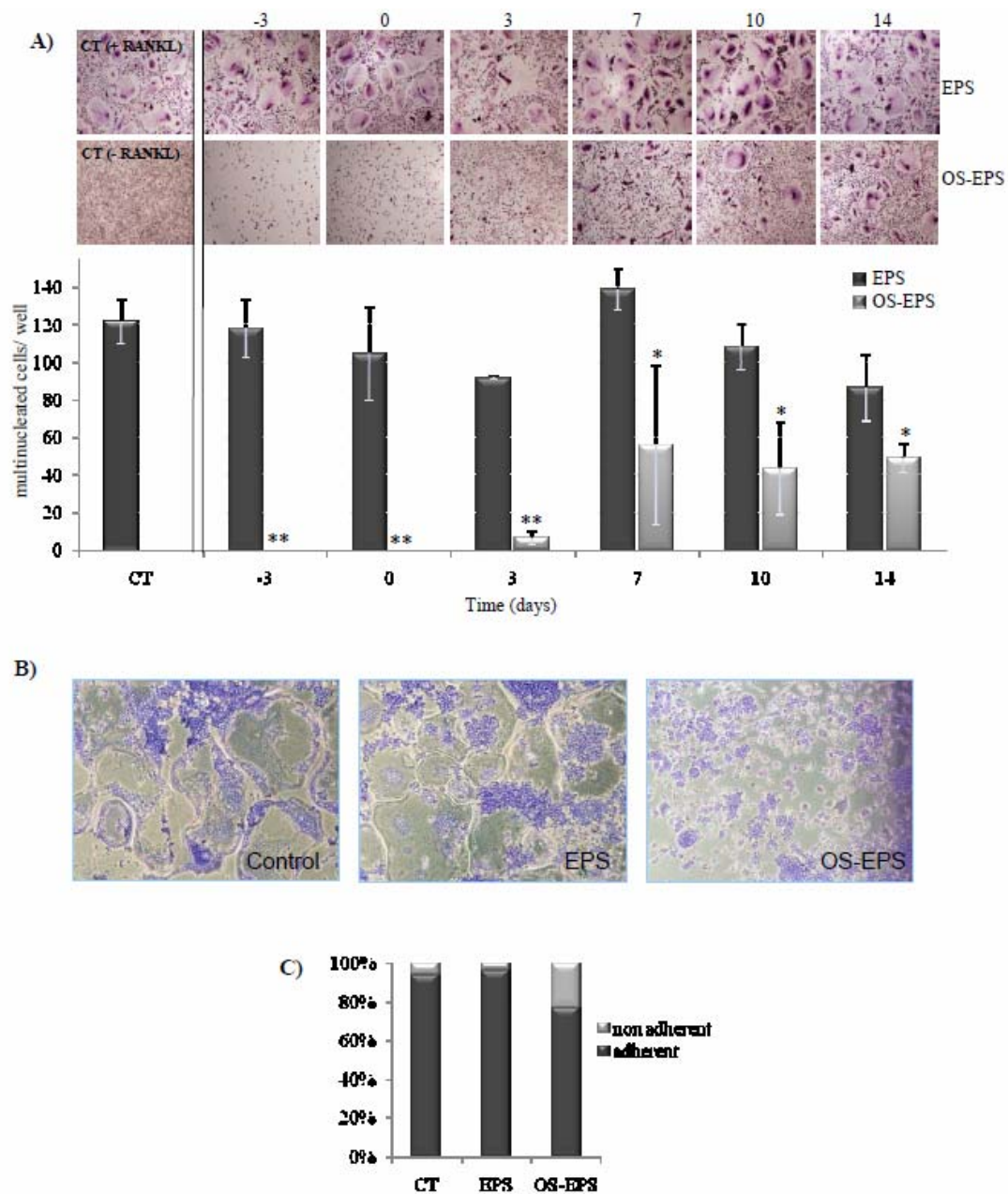


Figure 4: OS-EPS inhibits RANKL-induced osteoclastogenesis and cell adhesion of human CD14⁺ monocytes. (A) CD14⁺ purified monocytes were first cultured for 3 days in 25 ng/ml hM-CSF to attain complete cell adhesion. For osteoclastogenesis experiments, the cells were then incubated for 15 days in the presence of 25 ng/ml hM-CSF with or without hRANKL (100 ng/ml). EPS or OS-EPS (0.5 µg/ml) were added at different time points during the culture period, as indicated: -3 days indicates the culture condition with only 25 ng/ml of hM-CSF (cellular adhesion period); 0→14 days indicates the period with 25 ng/ml of hM-CSF and 100 ng/ml of RANKL (Osteoclastic differentiation period). At the end of the culture period, TRAP staining was performed (original magnification x 40) and TRAP positive multinucleated cells (more than 3 nuclei) were counted under a light microscope. (B) RAW 264.7 cells were cultured in the presence of hRANKL (100 ng/ml) and EPS or OS-EPS (0.5 µg/mL). After 5 days, the cells were stained for TRAP expression. (C) For adherence experiments, the cells were incubated for 5 days in the presence of EPS or OS-EPS at 1 µg/ml. The non-adherent cells in the supernatant were counted in triplicate by using blue trypan exclusion dye. The adherent cells were washed three times in 1x Dulbecco phosphate-buffered saline (DPBS), trypsinised and counted as above.

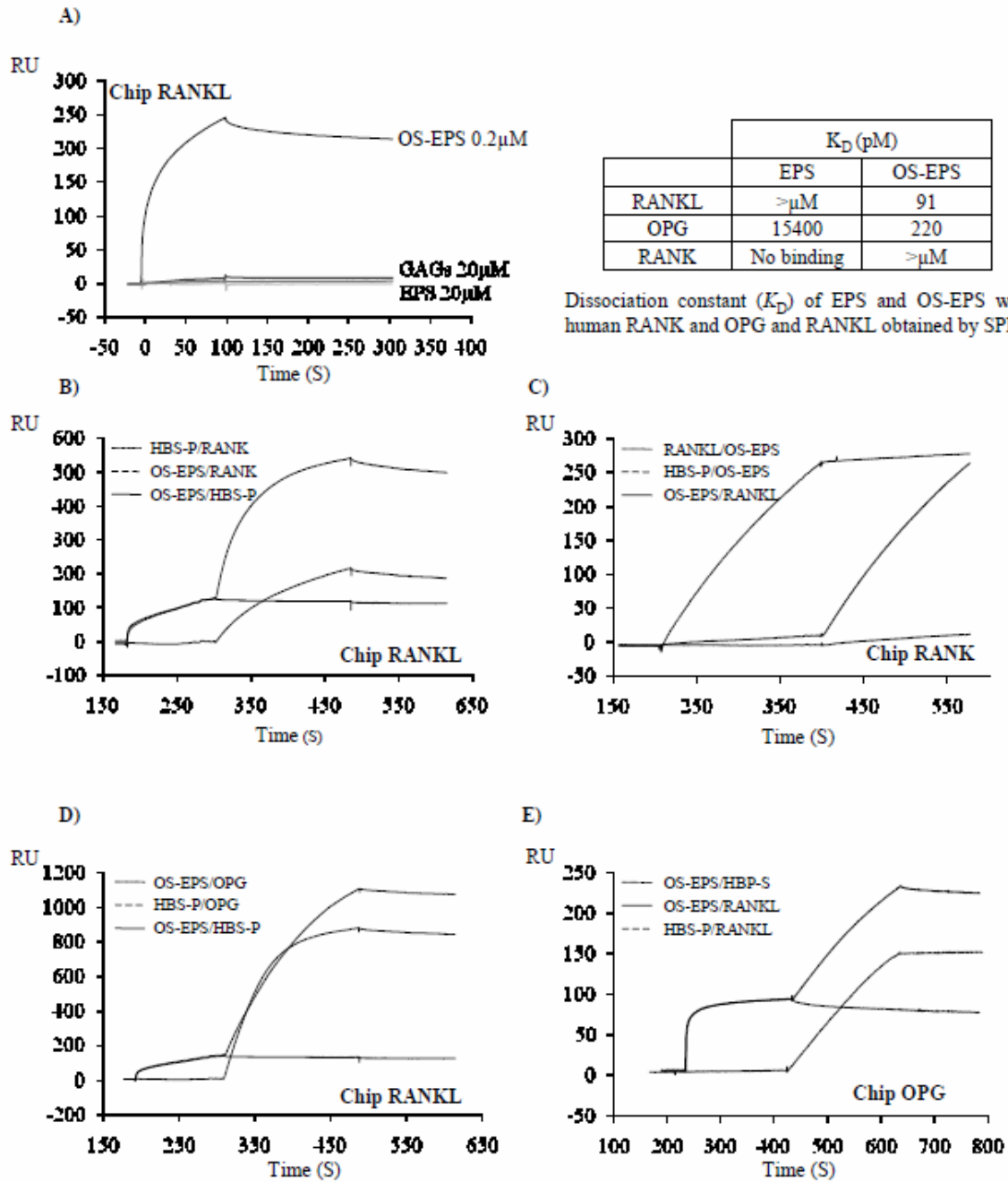


Figure 5: OS-EPS binds RANKL. Experiments were carried out on a BIAcore 3000 instrument (BIAcore). GAGs (20 μ M), or EPS (20 μ M), or OS-EPS (2 μ M) were injected at a flow rate of 30 μ l/min over the immobilized-RANKL sensorchip (A). Binding assays were performed at 25°C in 10 mM Hepes buffer, pH 7.4, containing 0.15 M NaCl and 0.005% P20 surfactant (HBS-P buffer, BIAcore). RANK (2 μ g/ml), or RANKL (0.5 μ g/ml) or OS-EPS (200nM) or OPG (1 μ g/ml) were injected at a flow rate of 30 μ l/min over the immobilized-RANKL sensorchip (B, D) or over the immobilized-RANK (C) or over the immobilized-OPG (E). EPS and OS-EPS K_D values for immobilized OPG, RANK and RANKL were assessed (Table).

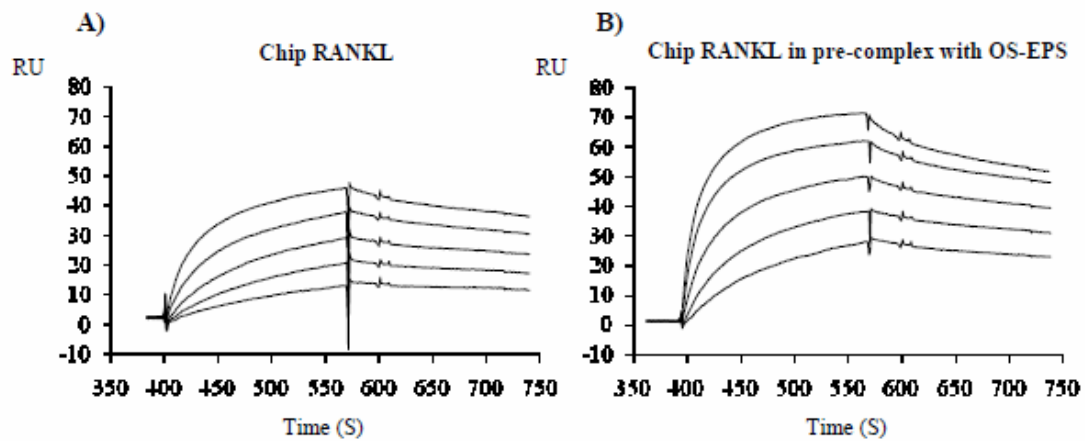


Figure 6: OS-EPS facilitates the binding of RANK-RANKL. Real-time SPR binding analyses of interactions between RANK and RANKL pre-incubated or not with OS-EPS. Sensorgrams were recorded with RANKL (A) or RANKL pre-incubated with OS-EPS (B) immobilized on CM5 sensor chips, and injections of RANK solutions [50, 25, 12.5, 6.25, and 3.125 nM RANK], using a BIAcore 3000 biosensor and BiaEval 4.1 software. The kinetic and thermodynamic values were k_a ($M^{-1}s^{-1}$) = $5.28 \cdot 10^5$; k_d (s^{-1}) = $1.27 \cdot 10^{-3}$ and K_D = 2.39 nM for RANKL in (A), and k_a ($M^{-1}s^{-1}$) = $1.23 \cdot 10^6$; k_d (s^{-1}) = $1.32 \cdot 10^{-3}$ and K_D = 1.09 nM for RANKL pre-incubated with OS-EPS in (B).

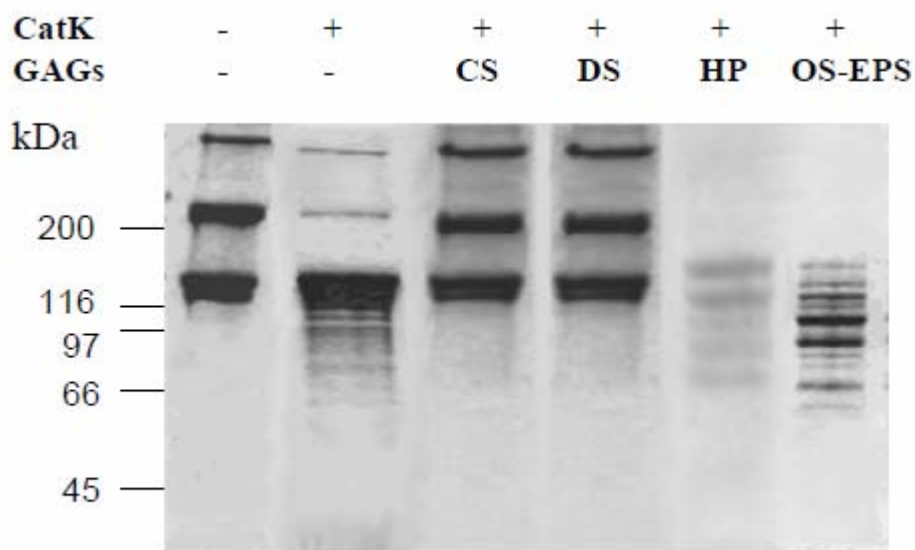


Figure 7: OS-EPS increases the collagenolytic activity of cathepsin K at physiological plasma pH. 0.5 mg/ml Calf-skin collagen was incubated with 0.25 μ M cathepsin K (CatK) in the presence or absence of different GAGs or OS-EPS for 12 h at 25°C. Polypeptides were separated by SDS/PAGE (8%gels) and stained with Coomassie Brilliant Blue R-250.

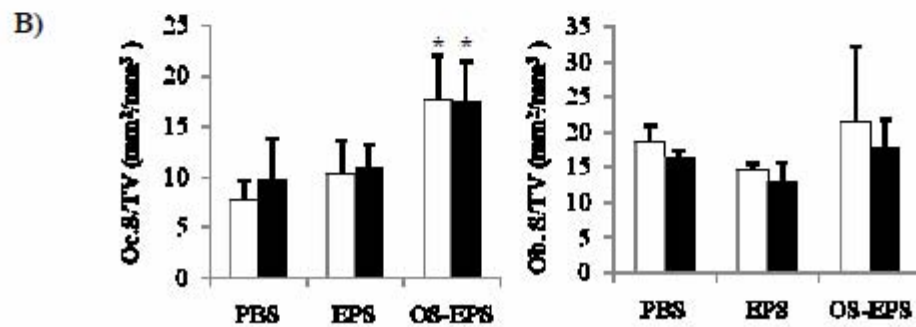
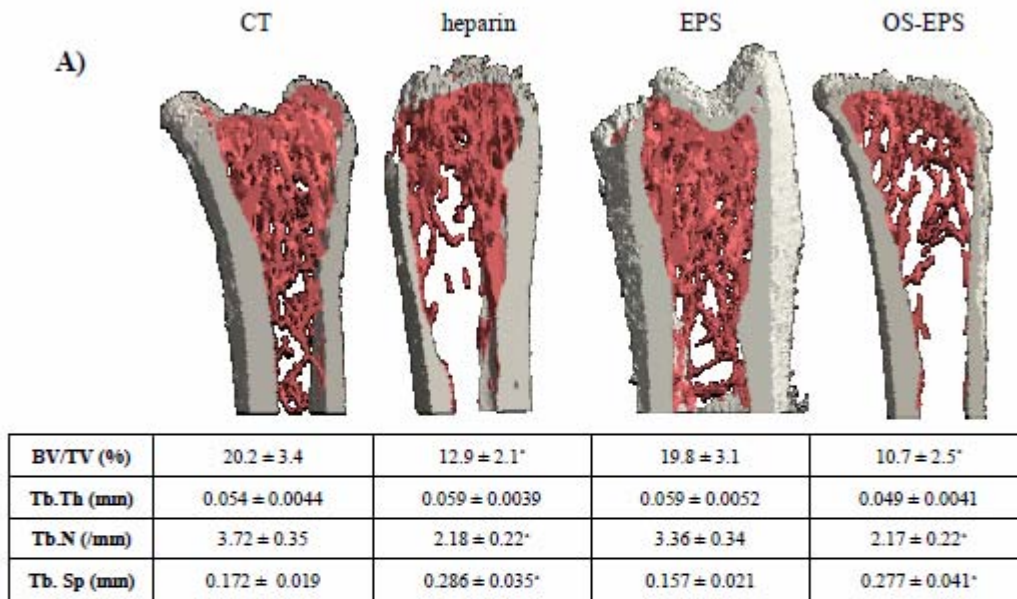


Figure 8: OS-EPS reduces trabecular bone. Twenty-four 4-week-old male C3H/HeN mice received a daily s.c. injection of DPBS, EPS, OS-EPS or heparin (6 mg/kg) for a period of 28 days. **(A)** The right femur from each animal was dissected for micro-architectural parameter quantification. The distal metaphyses were used for micro-computed tomography (μ -CT) on a SkyScan-1072 (SkyScan, Aartselaar, Belgium). μ CT-Analyser software SkyScan was used to analyse the structure of the samples. Bone volume ratio (BV/TV), trabecular thickness (Tb.Th), trabecular number (Tb.N) and trabecular separation (Tb.Sp) were assessed (**Table**). (n= 6 per group). (*: p < 0.05). **(B)** Analysis and quantification of osteoblastic and osteoclastic areas were done using a Leica Q500 image analysis system after TRAP and ALP staining, respectively. Two independent experiments were performed (n= 6 by groups). (*: p < 0.05).

Table 1: Primer sequence for osteogenic markers and RANKL

Gene	Gene (full name)	Accession N°	Sequence	(5'→3')
ALP	Alkaline phosphatase	NM_013059.1	Forward: Reverse:	aggggcaactccattttg ttgaaccaggcccgtg
Runx2	runt-related transcription factor 2	NM_053470.1	Forward: Reverse:	cacagagctattaaagtgacagtgg aacaactaggttagagtcatacaagc
BSP	Bone Sialoprotein	NM_012587.2	Forward: Reverse:	cctactttatcctcctctgaaacg tcgcatctccattttctc
OC	Osteocalcin	NM_013414.1	Forward: Reverse:	aagcgcatctatggcaccac tcgagtcctggagagtagcc
Collα1	Alpha-1 type I collagen	NM_053304.1	Forward: Reverse:	catgttcagctttgtggacct gcagctgacttcagggatgt
Cyc1 RANKL	cytochrome c-1	NM_001130491.1	Forward: Reverse:	tgctacacggaggaagaagc atcctcattagggccatcct
	tnfsf11 (Mus musculus)	NM_011613.3	Forward: Reverse:	agacacagaagcactactctgactc ggccccacaatgtgtgta